pp 1145–1162. © Royal Aeronautical Society 2018
doi: 10.1017/aer.2018.40

Cruise missile head shape optimisation using an adaptive sampling surrogate model

S. Z. Guo
szguo@nuaa.edu.cn
X. M. Zheng and H. S. Ang
Nanjing University of Aeronautics & Astronautics
Baixia, Nanjing
China

H. M. Cai
Nanjing University of Science and Technology
Qinhuai, Nanjing
China

ABSTRACT

High-precision response of the surrogate model is desired in the process of optimisation. An excessive number of sampling points will increase the cost of the calculation. The appropriate number of sampling points cannot only guarantee the accuracy of the surrogate model but also save the calculation cost. The purpose of this research is to demonstrate the eventuality of using an adaptive surrogate model for optimisation problems. The adaptive surrogate model is built on an adaptive sampling approach and an extended radial basis function (ERBF). The adaptive sampling is an approach that new sampling points are placed in the blank area and all the sampling points are uniformly distributed in the design region using Multi-Island GA. The precision of the ERBF surrogate model is checked using standard error measure to determine whether the surrogate model should be updated or not. This adaptive surrogate model is used to optimise a cruise missile head shape. Aerodynamic and stealthy performance of the cruise missile head shape are considered in this research. Different global objective function and different weight factor are used to research the aerodynamic and stealthy performance in this optimisation process. The results show that the drag is reduced with a slender head shape and the radar-cross section (RCS) value is reduced with a short head shape.

Keywords: Extended radial basis function; adaptive sampling; surrogate model; optimisation; cruise missile

Received 10 October 2017; revised 15 March 2018; accepted 16 March 2018; first published online 8 May 2018.

NOMENCLATURE

c, γ, n	prescribed parameter
ERBF	extended radial basis function
LHS	Latin hypercube sampling
n_p	the number of sampling points
RBF	radial basis function
RSM	response surface methodology
w_i	weight factor
x	the coordinates of the sampling point
x^i	the coordinates of the sampling point x^i
x_j	point x along the $j-$th dimension
x_j^i	point x_j along the $j-$th dimension
$\sigma_i, \alpha_{ij}^L, \alpha_{ij}^R, \beta_{ij}^L$	unknown factor

1.0 INTRODUCTION

Researchers make heavy use of computer simulation codes to replace expensive physical experiments and improve the quality and performance of engineered products and devices in many science and engineering fields. Such simulation activities are collectively referred to as *computational science* or *engineering*. Unfortunately, while allowing scientists more flexibility to study the phenomena under controlled conditions, computer simulations require a substantial investment on computation time. One simulation may take many minutes, hours, days or even weeks, quickly rendering parameter studies impractical[1-3]. To meet the challenge of increasing model complexity, the process of building approximate models, or surrogate model, has gained wide acceptance from the design community[4-6]. Such surrogate models have been successfully applied to optimisation problems[7,8]. Among the available surrogate model techniques, the Response Surface Methodology (RSM) approach was introduced by Box and Wilson in 1951[9]. This approach was used to optimise fire performance of ultra-low density fiberboards polynomial by Wu[10] in 2017. Kriging approach was named by French mathematician Matheron in 1963, after the South African mining engineer Krige, as it is still known in spatial statistics today. The Kriging approach is used to optimise the structure of water axial piston pump and cavitation of plunger cavity in 2016[11]. Radial basis function (RBF) methods are effective multi-dimensional approximation approaches. The performances of RBF methods are independent of the dimensionality to an extent[12]. An approach of extended radial basis function (ERBF) is proposed by Mullur and Messac[13] in 2005. The ERBF approaches are more flexible compare with RSM, Kriging and RBF. Since the ERBF approach is used to build the surrogate model in this research. However, these surrogate model approaches are all have no adaptive capability to the sampling points chosen. In the field of adaptive sampling techniques, Chen[14] used a local adaptive sampling to enhance the efficiency of constructing Kriging models for reliability-based design optimisation problems in 2014. But this approach is not applicable if sampling points are close to the limit state boundaries. An adaptive importance sampling techniques based on stochastic Newton recursions was used to accurately predict the power penalty induced[15]. Li, Wuand Chuang[16] apply Stein's Unbiased Risk Estimator (SURE) to adaptive sampling and reconstruction to reduce noise in Monte Carlo rendering. Aerodynamic shape of high-speed train nose is optimised using the adaptive surrogate model[17]. An approach for

https://doi.org/10.1017/aer.2018.40 Published online by Cambridge University Press

constructing adaptive surrogate models with application in production optimisation problem is proposed[18]. However, these approaches are not applicable, considering that increases new sampling points in the blank region after initial training points are selected using Latin hypercube sampling (LHS). A stochastic process model is proposed by Jones, Schonlau and Welch[19] based on response surface methodology in 1998. This stochastic process model is widely used in global optimisation. This approach can be used to construct an efficient global optimisation algorithm with a credible stopping rule. However, the aim of this research is to find sample points with the lowest computational cost under specified accuracy. An adaptive sampling approach that new sampling points are placed in the blank area and all the sampling points are uniformly distributed in the design region is used. The Euclidean distances between new sampling points and selected sampling points are evaluated to locate where the new points should be using Multi-Island GA. This adaptive sampling approach combines with ERBF surrogate model is used to optimise aerodynamic and stealthy performance for a cruise missile head shape.

The remainder of the paper is organised as follows. In Section 2, the introduction to methods of optimisation and ERBF is provided. The adaptive surrogate model is built using a novel adaptive sampling approach and ERBF. In Section 3, a cruise missile head shape is optimised using the adaptive surrogate model, and some results are described. In Section 4, our contributions are briefly summarised.

2.0 RESEARCH METHOD

The process of aerodynamic and stealthy optimisation for cruise missile head is divided into two steps in this paper. The first step is to build an adaptive surrogate model. The second step is to combine the adaptive surrogate model with Multi-Island genetic algorithm to determine the optimum shape of the cruise missile head. The first step will be described in this section.

2.1 Optimisation methods

There are several meaningful optimisation methods in the optimised research field but one of the most used algorithms in engineering is the Genetic Algorithm (GA). Genetic algorithms are classical stochastic optimisation algorithms inspired by evolutionary analogy. Because of their robustness and ease of application, genetic algorithms are used for machine learning, automatic control, and so on. Instead of the traditional genetic algorithm, Multi-Island GA is employed for optimisation. In Multi-Island GA, the population is divided into several sub-populations staying on isolated "islands", whereas traditional genetic algorithm operations are performed on each sub-population separately. A certain number of individuals between the islands migrate after a certain number of generations. Thus, Multi-Island GA can prevent the problem of "premature" by maintaining the diversity of the population[20]. In addition, the calculation speed of Multi-Island GA can be greater than that of traditional genetic algorithms.

2.2 Extended radial basis function models

The computer simulations to study and analyse designs are usually very expensive. In order to achieve the result, many computational resources and lots of time are needed. Since the problem of simulation cost becomes more severe. ERBF surrogate model-based design optimisation helps in reducing the number of real computer simulations necessary to solve this problem.

https://doi.org/10.1017/aer.2018.40 Published online by Cambridge University Press

ERBF approaches are the extension of RBF. RBF is expressed according to the Euclidean distance ($r = \|x - x^i\|$) of a generic point x from a given point data x^i which can be mathematically defined as

$$\varphi(r) = \sqrt{r^2 + c^2}, \quad \ldots (1)$$

where c is a prescribed parameter. The radial basis function is a linear combination equation, as described by

$$f(x^k) = \sum_{i=1}^{n_p} \sigma_i \varphi\left(\left\|x^k - x^i\right\|\right), \quad k = 1, ..., n_p, \quad \ldots (2)$$

where σ_i is the unknown factor to be solved and n_p represents the number of sampling points. The preceding equation is expressed in matrix form as follows:

$$\boldsymbol{A} \times \boldsymbol{\sigma} = \boldsymbol{F}, \quad \ldots (3)$$

where A_{ik}, $\boldsymbol{\sigma}$, $\boldsymbol{F}$ are written as

$$A_{ik} = \varphi\left(\left\|x^k - x^i\right\|\right), \quad i = 1, ..., n_p, k = 1, ..., n_p, \quad \ldots (4)$$

$$\boldsymbol{\sigma} = \left[\sigma_1 \sigma_2 ... \sigma_{n_p}\right]^T, \quad \ldots (5)$$

$$\boldsymbol{F} = \left[f(x^1) f(x^2) ... f(x^{n_p})\right]^T, \quad \ldots (6)$$

where A_{ik} is calculated by the Euclidean distance of point x^k and point x^i. The vector $\boldsymbol{\sigma}$ are defined by solving Equation (3). The Euclidean distances that unknown point x in the design domain relative to all date points (x^1, x^2, ..., x^{np}) into

$$\boldsymbol{\varepsilon} = \left[\varphi\left(\left\|x - x^1\right\|\right) \varphi\left(\left\|x - x^2\right\|\right) ... \varphi\left(\left\|x - x^{n_p}\right\|\right)\right] \quad \ldots (7)$$

The interpolation result of RBF for the generic point x is expressed as

$$f(x) = \boldsymbol{\varepsilon} \times \boldsymbol{\sigma} \quad \ldots (8)$$

The typical RBF approaches provide only an interpolative solving method to the surrogate model problem, but they do not provide patterns for the designer to deliver desirable performance for the meta-models. Mullur and Messac proposed a surrogate model of extended radial basis function[13]. They defined a coordinate vector as $\xi_j^i = x_j - x_j^i$, which is the coordinate of any point x in the design domain relative to the sampling point x^i along the $j-$ th dimension, and defined non-radial basis function as

$$\phi_{ij}(\xi_j^i) = \alpha_{ij}^L \phi^L(\xi_j^i) + \alpha_{ij}^R \phi^R(\xi_j^i) + \beta_{ij}^L \phi^\beta(\xi_j^i), \quad \ldots (9)$$

with the functions ϕ^L, ϕ^R and ϕ^β as described in Table 1.

https://doi.org/10.1017/aer.2018.40 Published online by Cambridge University Press

Table 1
The description of non-radial basis functions

$\boldsymbol{\xi_j^i}$	$\boldsymbol{\phi^L}$	$\boldsymbol{\phi^R}$	$\boldsymbol{\phi^\beta}$
$\xi_j^i \le -\gamma$	$(-n\gamma^{n-1})\xi_j^i + \gamma^n(1-n)$	0	ξ_j^i
$-\gamma \le \xi_j^i \le 0$	$(\xi_j^i)^n$	0	ξ_j^i
$0 \le \xi_j^i \le \gamma$	0	$(\xi_j^i)^n$	ξ_j^i
$\xi_j^i \ge \gamma$	0	$(n\gamma^{n-1})\xi_j^i + \gamma^n(1-n)$	ξ_j^i

where γ and n are prescribed parameters, extended radial basis function method is a surrogate model approach that combines radial with non-radial basis functions. It can be expressed as

$$f(x^k) = \sum_{i=1}^{n_p} \sigma_i \varphi\left(\left\|x^k - x^i\right\|\right) + \sum_{i=1}^{n_p} \phi_i (x^k - x^i) \quad \ldots(10)$$

and also

$$f(x^k) = \sum_{i=1}^{n_p} \sigma_i \varphi\left(\left\|x^k - x^i\right\|\right) + \sum_{i=1}^{n_p}\sum_{j=1}^{m} \left\{\alpha_{ij}^L \phi^L(\xi_j^i) + \alpha_{ij}^R \phi^R(\xi_j^i) + \beta_{ij}^L \phi^\beta(\xi_j^i)\right\}, \quad \ldots(11)$$

define:

$$\boldsymbol{\alpha^L} = \left\{\alpha_{11}^L \alpha_{12}^L \ldots \alpha_{1m}^L \ldots \alpha_{(n_p)(m)}^L\right\}_{(mn_p)(1)}^T, \quad \ldots(12)$$

$$\boldsymbol{\alpha^R} = \left\{\alpha_{11}^R \alpha_{12}^R \ldots \alpha_{1m}^R \ldots \alpha_{(n_p)(m)}^R\right\}_{(mn_p)(1)}^T, \quad \ldots(13)$$

$$\boldsymbol{\beta} = \left\{\beta_{11}\beta_{12}\ldots\beta_{1m}\ldots\beta_{(n_p)(m)}\right\}_{(mn_p)(1)}^T \quad \ldots(14)$$

so $f(x^k)$ is expressed as

$$\boldsymbol{A} \times \boldsymbol{\sigma} + \boldsymbol{B} \times \left\{(\boldsymbol{\alpha^L})^T (\boldsymbol{\alpha^R})^T \ \boldsymbol{\beta}^T\right\}^T = \boldsymbol{F}, \quad \ldots(15)$$

where the $k-$th row of $\boldsymbol{B}$ is expressed as

$$\boldsymbol{B^k} = \left\{\boldsymbol{B^{Lk}} \ \boldsymbol{B^{Rk}} \ \boldsymbol{B^{\beta k}}\right\}_{(1)\times(3mn_p)}, \quad \ldots(16)$$

where $\boldsymbol{B^{Lk}}$ is expressed as

$$\boldsymbol{B^{Lk}} = \left[\phi^L(x_1^k - x_1^1)\phi^L(x_2^k - x_2^1)\ldots\phi^L(x_m^k - x_m^1)\ldots\phi^L(x_m^k - x_m^{n_p})\right]_{(1)\times(mn_p)} \quad \ldots(17)$$

define

$$\overline{\boldsymbol{A}} = [\boldsymbol{A} \ \boldsymbol{B}] \quad \ldots(18)$$

https://doi.org/10.1017/aer.2018.40 Published online by Cambridge University Press

$$\overline{\boldsymbol{\alpha}} = \left\{ \boldsymbol{\sigma}^{\boldsymbol{T}} \quad \left(\boldsymbol{\alpha}^{\boldsymbol{L}}\right)^{T} \quad \left(\boldsymbol{\alpha}^{\boldsymbol{R}}\right)^{T} \quad \boldsymbol{\beta}^{T} \right\}^{T} \qquad \ldots (19)$$

so Equation (15) is expressed as

$$\overline{\boldsymbol{A}} \times \overline{\boldsymbol{\alpha}} = \boldsymbol{F} \qquad \ldots (20)$$

The vector $\overline{\boldsymbol{\alpha}}$ is defined by solving the Equation (20). The Euclidean distances and non-radial basis values that sampling point x relative to all data points (x^1, x^2, …, x^{np}) into

$$\begin{aligned} \bar{\varepsilon} = \big[& \varphi\left(\left\|x - x^1\right\|\right) \quad \varphi(\left\|x - x^2\right\|) \ldots \varphi\left(\|x - x^{n_p}\|\right) \\ & \phi^L(x_1 - x_1^1) \quad \phi^L(x_2 - x_2^1) \ldots \phi^L(x_m - x_m^1) \ldots \phi^L(x_m - x_m^{n_p}) \\ & \phi^R(x_1 - x_1^1) \quad \phi^R(x_2 - x_2^1) \ldots \phi^R(x_m - x_m^1) \ldots \phi^R(x_m - x_m^{n_p}) \\ & \phi^\beta(x_1 - x_1^1) \quad \phi^\beta(x_2 - x_2^1) \ldots \phi^\beta(x_m - x_m^1) \ldots \phi^\beta(x_m - x_m^{n_p}) \big] \end{aligned} \qquad \ldots (21)$$

The interpolation result of ERBF for the generic point x can be expressed as

$$f(x) = \bar{\boldsymbol{\varepsilon}} \times \bar{\boldsymbol{\sigma}} \qquad \ldots (22)$$

The ERBF approaches provide the designer with significant flexibility and freedom compared with conventional RBFs in the surrogate model construction process, and their research results show that the ERBF approaches are more accurate in some research field[13].

To measure the surrogate model accuracy of the results, the standard error measure is used: Normalised root-mean-squared error (*NRMSE*). The error measure is defined as follows:

$$NRMSE = \left\{ \frac{\sum_{k=1}^{K} \left[f(x^k) - f(x^k)_{ERBF} \right]^2}{\sum_{k=1}^{K} \left[f(x^k) \right]^2} \right\}^{\frac{1}{2}} \times 100 \qquad \ldots (23)$$

The descriptive error measure represents the error level of the adaptive surrogate model. A tiny value of *NRMSE* indicates a good fit, whereas a high value of *NRMSE* indicates a poor fit. This standard error measure as convergence criteria to judge whether the iteration is converged or not.

2.3 An adaptive surrogate model for multi-objective optimisation problem

The adaptive surrogate model is built on an adaptive sampling approach and an extended radial basis function (ERBF) in our recent study[21]. We get the same surrogate model accuracy with minimal time and resources using this approach. The adaptive sampling is an approach in which new sampling points are placed in the blank area and all the sampling points are uniformly distributed in the design region using Multi-Island GA. The flow chart of the adaptive surrogate model approach for the aerodynamic and stealthy multidisciplinary optimisation is shown in Fig. 1. The original sampling points for the ERBF surrogate model building is picked using the LHS technique. These original sampling points are used for

https://doi.org/10.1017/aer.2018.40 Published online by Cambridge University Press

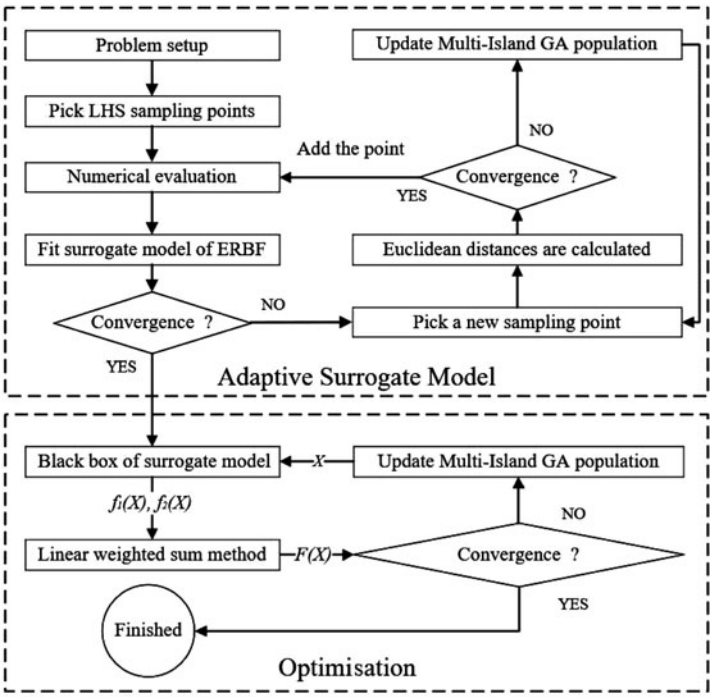

Figure 1. Flow chart showing the multi-objective optimisation process.

aerodynamic and stealthy numerical evaluation, and the results of numerical evaluation are used to fit the surrogate model of ERBF. Standard error measure as convergence criteria to judge whether the iteration is converged or not. A new sampling point is searched using the Multi-Island GA technique. This new sampling point is added to the numerical evaluation if the convergence condition is not satisfied. The Euclidean distances between the new sampling point and the selected sampling points are evaluated during the process of searching new sampling point. The new sampling point is added to the numerical evaluation if the iteration is convergent in the process of searching new sampling point. Otherwise, update the Multi-Island GA population. Black box of surrogate model is fitted if the convergence condition is satisfied. The black box of the surrogate model is used to find the response in the multi-objective optimisation. For this multi-objective optimisation problem, the linear weighted sum method is employed as follows:

$$\text{Maximum} \quad F(X) = \sum_{i=1}^{m} w_i f_i(X) \qquad \ldots (24)$$

$$\text{Subject to} \quad e(X) = (e_1(X), e_2(X), ..., e_m(X)) \leq 0 \qquad \ldots (25)$$

Go to finished if the iteration is converged; otherwise, update the Multi-Island GA population.

The adaptive sampling approach is illustrated by a sampling case of two design variables. The circular points are the initial sampling points, and the square points from 1 to 11 are ready to add to the numeral calculations in Fig. 2. The square points are selected by the adaptive

https://doi.org/10.1017/aer.2018.40 Published online by Cambridge University Press

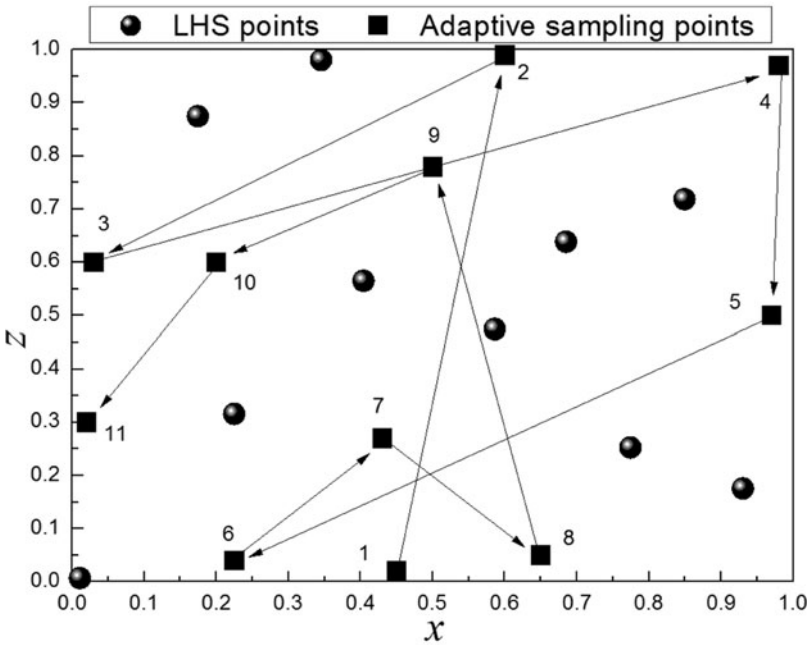

Figure 2. A case of the adaptive sampling approach.

sampling approach. Points 1, 2, ..., 11 are selected one by one using the Multi-Island GA. Point 1 is selected first, because the minimum Euclidean distance of Point 1 to all initial sampling points is maximum compared to Points 2, 3,..., 11. New sampling points are placed in the blank area and all the sampling points are uniformly distributed in the design region using the adaptive sampling approach. So the most appropriate sample points are chosen to improve the precision of the surrogate model.

3.0 AERODYNAMIC AND STEALTHY OPTIMISATION FOR A CRUISE MISSILE HEAD USING THE ADAPTIVE SURROGATE MODEL

In the aerodynamic and stealthy design process for cruise missile head, the aerodynamic drag and the RCS value should be reduced. This is a multidisciplinary optimisation problem. In this section, the aerodynamic characteristics and the radar target characteristics of the cruise missile head are considered, and aerodynamic and stealthy optimisation for the cruise missile head is studied using the adaptive surrogate model and Multi-Island GA algorithm.

3.1 CAD model of cruise missile head and numeral calculations

The shape of the cruise missile head is shown in Fig. 3. The shape is controlled by the control point. In order to ensure the control point is not too low or high, the maximum value of z is equal to 270 mm. The minimum value of z is equal to 0 mm. For the purpose of the cruise missile head size is not too long or too short. The maximum of x is equal to 1500 mm, and the

https://doi.org/10.1017/aer.2018.40 Published online by Cambridge University Press

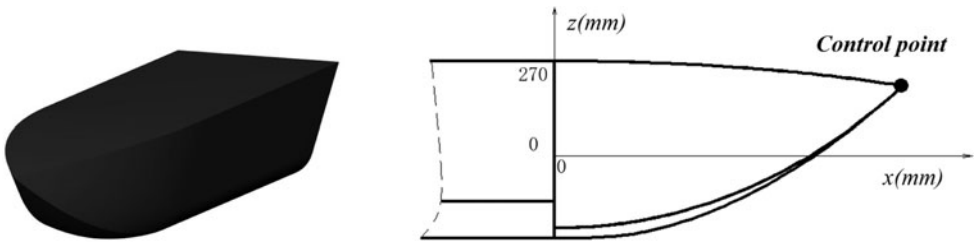

Figure 3. Geometrical parameters of the cruise missile head.

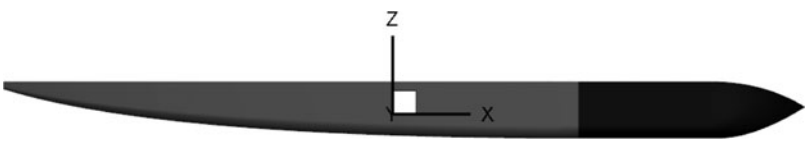

Figure 4. CAD model of complete aircraft fuselage for CFD numerical calculation.

minimum of x is equal to 500 mm. The shape of the cruise missile head ensures that the curve and the surface are smooth.

The velocity of the cruise missile is equal to 0.65 M. The flying height is equal to 6000 m. In order to ensure that the subsonic CFD numerical calculation is correct, a complete aircraft fuselage is used as shown in Fig. 4. However, we only monitor the drag of the cruise missile head in the CFD numerical calculation.

According to the windward area of the cruise missile head and the air conditions, the value of the feature size is equal to 0.773 m, and the value of the Reynolds number is equal to 6.4×10^6. In the grid generation process, the thickness of the first layer of the boundary layer will have an impact on the drag. The value of $y+$is equal to 30. According to the boundary-layer empirical formula, the value of first layer thickness is equal to 0.0001 m. The grid of the cruise missile head is shown in Fig. 5. The number of grid cells is equal to 3 m. Velocity-inlet and pressure-outlet as the boundary conditions of the CFD calculation.

Because of the different power and wavelength of radar, the detection distance is different. The radar detection distance is up to 4000 km or more. In order to ensure that the cruise missile is not detected by the ground radar at cruise, the RCS of the missile head in the range of 0° to 5° should be small. So the pitch angle ranges from 0° to 5° in the RCS numerical calculation as shown in Fig. 6. A radar-wave frequency of 9 GHz as the input wave in the RCS numerical calculation. The calculation fields in the plane-wave incident direction only be considered. Horizontal polarization as the polarization direction. The RCS average value, which is calculated once every 0.1 degrees in the range from 0° to 5°.

3.2 Problem set-up

The Pareto front can be found using the Pareto ranking method in this research. However, the main issues we are concerned with are the drag coefficient and the RCS value, with the absolute value of the RCS value divided by the drag coefficient. Concerning the drag coefficient and the RCS value, the linear-weighted sum method is employed as follows:

$$F(X) = \frac{w_1 f_1(X) + w_2 f_2(X)}{w_1 + w_2}, \qquad \ldots (26)$$

https://doi.org/10.1017/aer.2018.40 Published online by Cambridge University Press

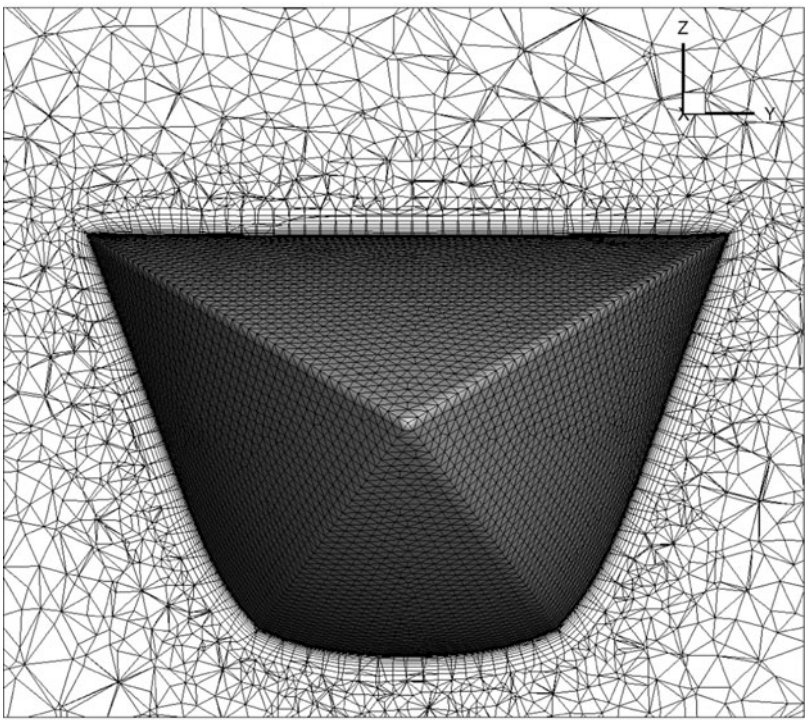

Figure 5. The grid of the cruise missile head.

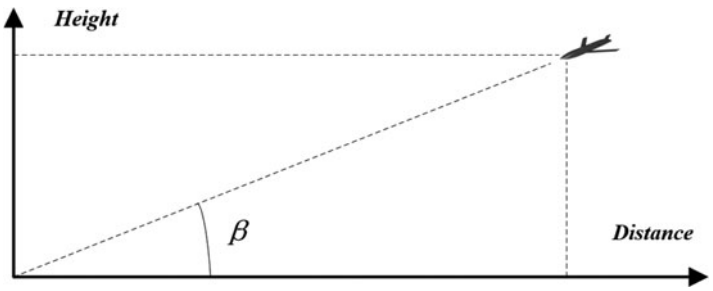

Figure 6. Range of pitch angle for the RCS numerical calculation ($0° < \beta < 5°$).

where $F(X)$ is the global objective function and $f_1(X)$ and $f_2(X)$ are the drag coefficient and the RCS value, respectively. The w_1 and w_2 are the weight factors. In order to more clearly distinguish between aerodynamic performance and stealth performance, two kinds of weight factors are only considered in this paper. One is that $w_1 = 1$ and $w_2 = 0$. Another one is that $w_1 = 0$ and $w_2 = 1$. The two kinds of weight factors consider aerodynamic performance and stealth performance, respectively. Concerning the absolute value of the RCS value divided by the drag coefficient, there is a global objective function as follows:

$$F(X) = \left| \frac{f_2(X)}{f_1(X)} \right| \quad \ldots (27)$$

https://doi.org/10.1017/aer.2018.40 Published online by Cambridge University Press

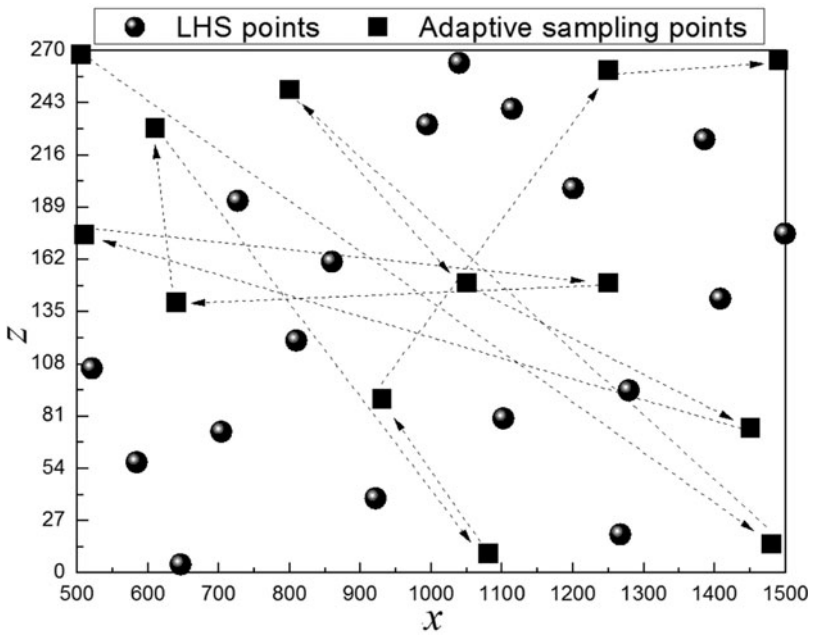

Figure 7. Distribution of sampling points.

The $f_2(X)$ is a negative number. The smaller the value of $f_2(X)$, the stronger the stealthy capability. The $f_1(X)$ is a positive number. The smaller the value of $f_1(X)$, the better the aerodynamic performance. Minimising the $F(X)$ for Equation 26, and maximising the $F(X)$ for Equation 27 is the direction in this optimisation.

The geometry constraints as follows:

$$500 \leq x \leq 1500, \quad \ldots (28)$$

$$0 \leq z \leq 270 \quad \ldots (29)$$

3.3 Results

The initial sampling points required to build the ERBF surrogate model are selected using the LHS approach. The whole number of 18 training points is picked to build the original surrogate model as shown in Fig. 7. The number of original training points may be fewer or more. The 18 training points selected here are artificially defined as examples. The adaptive algorithm is able to check the accuracy of the surrogate model by comparing the value of NRMSE and the request for additional sampling points whenever necessary. At 1.5% confidence bounds, the adaptive algorithm requested a supernumerary 13 sampling points to improve the accuracy of the ERBF surrogate model. The confidence bound of 1.5% is satisfied using a total of 31 sampling points.

The selection of the weights for the multi-objective functions will have a greater effect on the final optimum drag and RCS, since the weights will decide the locations of the optimum design variables[22]. Aerodynamic and stealthy optimisations are studied using different weights. The optimisation history of the multi-objective function with the first

https://doi.org/10.1017/aer.2018.40 Published online by Cambridge University Press

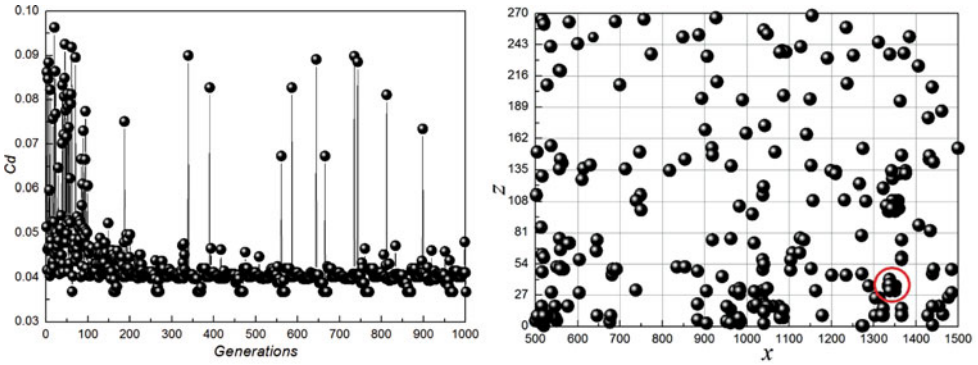

Figure 8. (Colour online) Optimisation history and distribution of control point for Equation 26, $w_1 = 1$, $w_2 = 0$, 1.5% NRMSE.

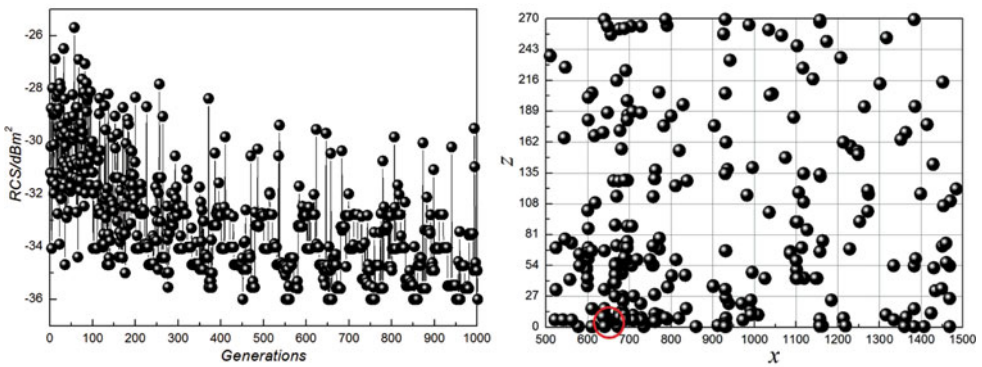

Figure 9. (Colour online) Optimisation history and distribution of control point for Equation 26, $w_1 = 0$, $w_2 = 1$, 1.5% NRMSE.

weights ($w_1 = 1$, $w_2 = 0$) for the first objective function (Equation 26) is illustrated in Fig. 8. The aerodynamic optimisation history shows the decrease of $F(X)$. The number of islands is equal to 10 in the Multi-Islands GA algorithm, since there are ten locally optimal solutions. But the globally optimal solution has only one, the value of $F(X)$ equal to 0.037. The values of x and z are equal to 1337.8 mm and 30.9 mm, respectively. The location of the control point is marked using a red circle in Fig. 8.

The optimisation history of the multi-objective function with the second weights ($w_1 = 0$, $w_2 = 1$) for the first objective function (Equation 26) is illustrated in Fig. 9. The stealthy optimisation history shows the decrease of $F(X)$. The number of islands is equal to 10 in the Multi-Islands GA algorithm, since there are ten locally optimal solutions. But the globally optimal solution has only one, the value of $F(X)$ equal to 35.8 dBm^2. The values of x and z are equal to 640.2 mm and 0.6 mm, respectively. The location of the control point is marked using a red circle in Fig. 9.

The optimisation history of the multi-objective function for the second objective function (Equation 27) is illustrated in Fig. 10. The aerodynamic and stealthy optimisation history shows the increase of $F(X)$. The number of islands is equal to 10 in the Multi-Islands GA algorithm, since there are ten locally optimal solutions. But the globally optimal solution has

https://doi.org/10.1017/aer.2018.40 Published online by Cambridge University Press

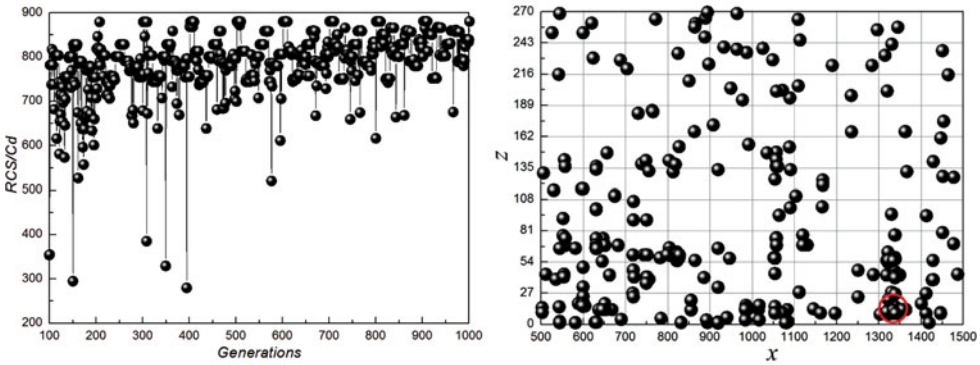

Figure 10. (Colour online) Optimisation history and distribution of the control point for Equation 27, 1.5% NRMSE.

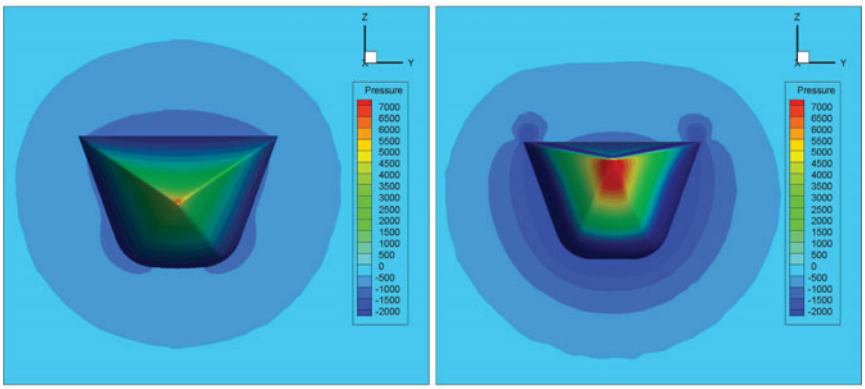

Figure 11. (Colour online) Comparison of the pressure distribution between the original model ($x = 800$ mm, $z = 200$ mm) and the optimised model ($x = 1337.8$ mm, $z = 30.9$ mm).

only one, the value of $F(X)$ equal to 880.6. The values of x and z are equal to 1339.3 mm and 9.6 mm, respectively. The location of control point is marked using a red circle in Fig. 10.

Stealthy and aerodynamic performance are researched between the original model and the optimised model in this section. In the original model, the values of x and z are equal to 800 mm and 200 mm, respectively. The value of w_1 equal to 1 and the value of w_2 equal to 0 in Equation 26 means that aerodynamic performance is considered only in the optimisation process. The cruise-missile-head pressure distributions of the original model and the optimised model are shown in Fig. 11. The left one is the pressure distribution of the optimised model ($x = 1337.8$ mm, $z = 30.9$ mm), and the right one is the pressure distribution of the original model ($x = 800$ mm, $z = 200$ mm). The high-pressure area of the original model is significantly larger than that of the optimised model. The drag coefficient of the optimised model is equal to 0.036 and the drag coefficient of the original model is equal to 0.064.

The cruise-missile-head streamlines of the original model and the optimised model are shown in Fig. 12. The left one is the streamline of the optimised model ($x = 1337.8$ mm, $z = 30.9$ mm), and the right one is the streamline of the original model ($x = 800$ mm, $z = 200$ mm). The airflow at the head of the cruise missile has been separated in the original

https://doi.org/10.1017/aer.2018.40 Published online by Cambridge University Press

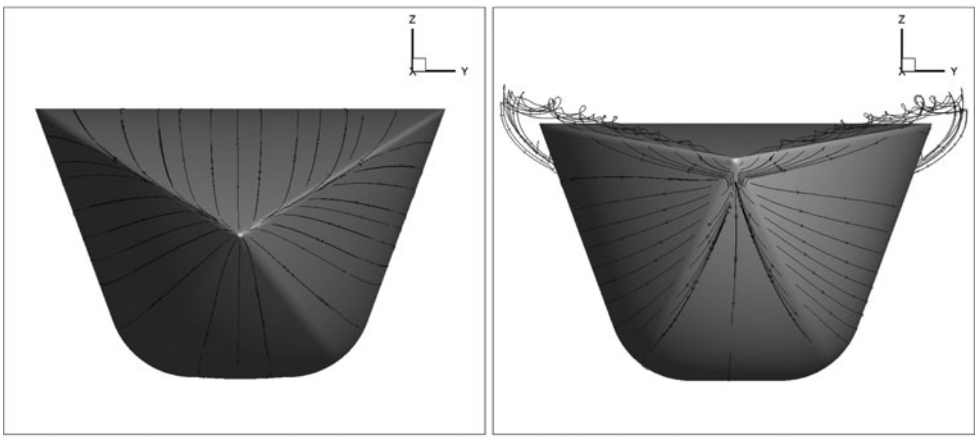

Figure 12. Comparison of streamline between the original model ($x = 800$ mm, $z = 200$ mm) and the optimised model ($x = 1337.8$ mm, $z = 30.9$ mm).

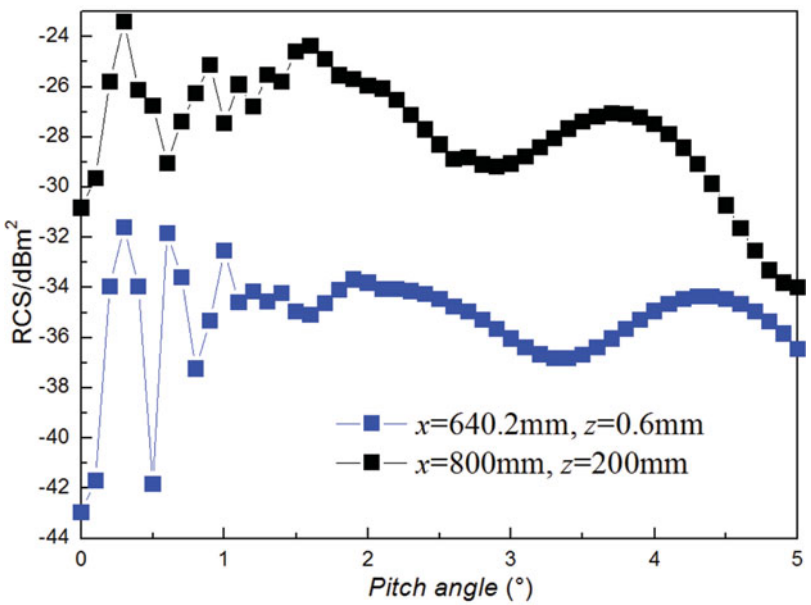

Figure 13. (Colour online) Comparison of RCS between the original model ($x = 800$ mm, $z = 200$ mm) and the optimised model ($x = 640.2$ mm, $z = 0.6$ mm).

model. The airflow at the head of the cruise missile is transferred smoothly in the optimised model.

The value of w_1 equal to 0 and the value of w_2 equal to 1 in Equation 26 means that stealth performance is considered only in the optimisation process. The RCS values of the original model and the optimised model are shown in Fig. 13. The blue line is the RCS value of the optimised model ($x = 640.2$ mm, $z = 0.6$ mm) and the black line is the RCS value of the original model ($x = 800$ mm, $z = 200$ mm). The blue line is under the black line completely.

https://doi.org/10.1017/aer.2018.40 Published online by Cambridge University Press

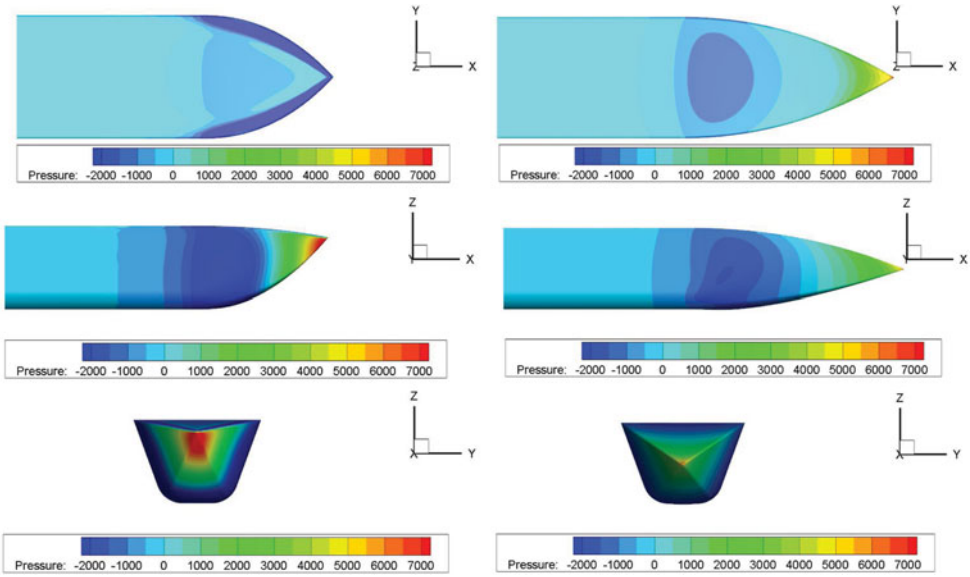

Figure 14. (Colour online) Comparison of the pressure distribution between the original model ($x = 800$ mm, $z = 200$ mm) and the optimised model ($x = 1339.3$ mm, $z = 9.6$ mm).

The RCS average value of the optimised model is equal to 35.8 dBm^2 and the RCS average value of the original model is equal to 31.7 dBm^2.

The global objective function (Equation 27) means that stealthy and aerodynamic performance are all considered in the optimisation process. The pressure distribution three-dimensional views of the original model and the optimised model are shown in Fig. 14. The left side is the pressure distribution three-dimensional view of the original model ($x = 800$ mm, $z = 200$ mm). The right side is the pressure distribution three-dimensional view of the optimised model ($x = 1339.3$ mm, $z = 9.6$ mm). The top view of the pressure distribution indicates that the airflow is separated in the original model and the airflow is smooth in the optimised model. The front view of the pressure distribution indicates that the high-pressure area of the original model is significantly larger than that of the optimised model. The drag coefficient of the optimised model is equal to 0.038.

The RCS values of the original model and the optimised model are shown in Fig. 15. The red line is the RCS value of the optimised model ($x = 1339.3$ mm, $z = 9.6$ mm) and the black line is the RCS value of the original model ($x = 800$ mm, $z = 200$ mm). The RCS average value of the optimised model is equal to -32.3 dBm^2.

The above results show that the choice of the weights for the multi-objective functions has a major effect on the final optimum results. The shape of optimised cruise missile head is shown in Fig. 16. When the optimised shape of the first weight factor (Equation 26, $w_1 = 1$, $w_1 = 0$) and the optimised shape of global objective function (Equation 27) are compared, we find that the two optimised shapes are similar. The value of x is equal to 1339.3 mm and the value of z is equal to 9.6 mm for the global objective function (Equation 27), and the value of x is equal to 1337.8 mm and the value of z is equal to 30.9 mm for the global objective function (Equation 26, $w_1 = 1$, $w_1 = 0$). But optimised shape of second weight factor (Equation 26, $w_1 = 0$, $w_1 = 1$) is different from the above two optimised shapes. The value of x is equal to

https://doi.org/10.1017/aer.2018.40 Published online by Cambridge University Press

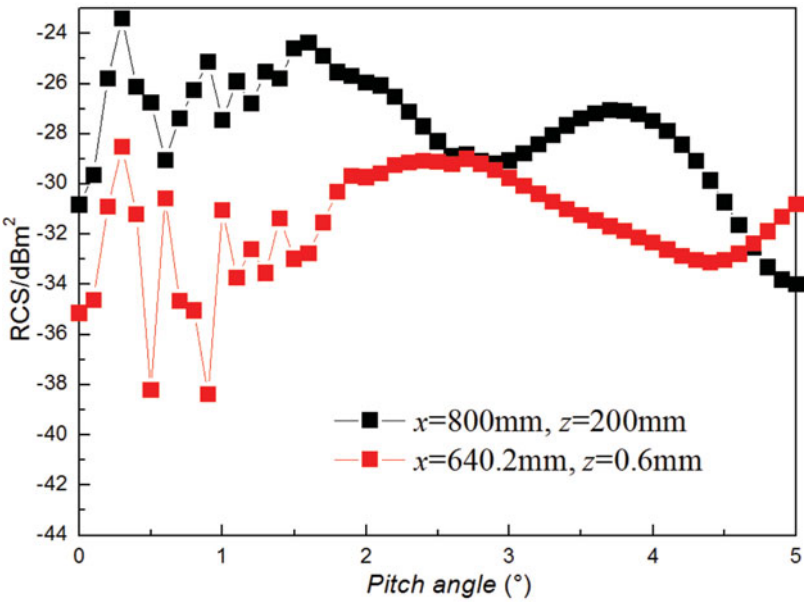

Figure 15. (Colour online) Comparison of RCS between the original model and the optimised model (Equation 27).

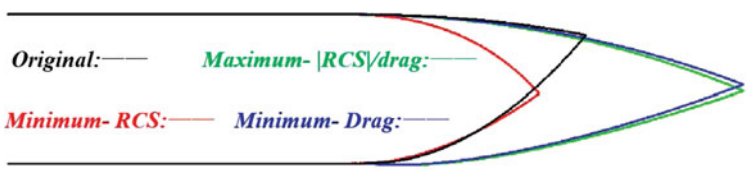

Figure 16. (Colour online) The shape of the optimised cruise missile head.

640.2 mm and the value of z is equal to 0.6 mm for the global objective function (Equation 26, $w_1 = 0$, $w_1 = 1$).

4.0 CONCLUSIONS

An adaptive sampling approach in which new sampling points are placed in the blank area and all the sampling points are uniformly distributed in the design region is used. Multi-objective optimisation of the cruise missile head shape by considering two objectives: drag coefficient and RCS value.

Minimising the drag coefficient and RCS value is performed using Multi-Island GA algorithm. The executable of optimising using the adaptive surrogate model in combination with Multi-Island GA optimisation approach is demonstrated successfully.

It is observed that a total of 18 LHS sampling points are picked to calculate the original ERBF surrogate model. The optimisation presented in this paper required 13 sampling points for 1.5% confidence bound.

The effect of the selection of different weights on the optimum cruise missile head shape is researched. Considering drag coefficient only, the drag coefficient is optimised to

https://doi.org/10.1017/aer.2018.40 Published online by Cambridge University Press

0.036. Considering RCS only, the value of RCS is optimised to $-35.8\,\mathrm{dBm}^2$. Considering drag coefficient and RCS all, the ratio of drag coefficient to the absolute value of RCS is optimised to 850, and the drag coefficient is optimised to 0.038, the value of RCS is optimised to $-32.3\,\mathrm{dBm}^2$.

ACKNOWLEDGEMENTS

Project supported by the Natural Science Foundation of Jiangsu Province, China (Grant No. BK20160817) and the Fundametnal Research Funds for the Central Universities (Grant No. 30915118807, 30917011302).

REFERENCES

1. FORRESTER, A.I.J., SÓBESTER, A. and KEANE, A.J. *Engineering Design via Surrogate Modelling: A Practical Guide*. DBLP, 2008.
2. DENG, S., PERCIN, M., VAN-OUDHEUSDEN, B.W., BIJL, H., REMES, B. and XIAO, T. Numerical simulation of a flexible x-wing flapping-wing micro air vehicle, *AIAA J*, 2017, **55**, (7), pp 2295-2306.
3. BRAUN, M., KLEDITZSCH, S. and SCHARLER, R. A method for reduction of computational time of local equilibria for biomass flue gas compositions in CFD, *Progress in Computational Fluid Dynamics, an Int J*, 2006, **6**, (4-5), pp 272-277.
4. BRAUN, U.M. and RIEDEL, U. Alternative fuels in aviation, *Aeronaut J*, 2015, **6**, (1), pp 83-93.
5. JOUHAUD, J.C., SAGAUT, P. and MONTAGNAC, M. A. Surrogate-model based multidisciplinary shape optimisation method with application to a 2D subsonic airfoil, *Computers & Fluids*, 2007, **36**, (3), pp 520-529.
6. QUEIPO, N.V., HAFTKA, R.T. and SHYY, W. Surrogate-based analysis and optimization, *Progress in Aerospace Sciences*, 2005, **41**, (1), pp 1-28.
7. ROSENOW, J., LINDNER, M. and FRICKE, H. Impact of climate costs on airline network and trajectory optimization: A parametric study, *Aeronaut J*, 2017, **8**, (2), pp 371-384.
8. CONWAY, B. A., ed. *Spacecraft Trajectory Optimization*. Cambridge University Press, 2010.
9. BOX, G.E.P. and WILSON, K.B. On the experimental attainment of optimum conditions, *Journal of the Royal Statistical Society*, 1951, **13**, (1), pp 1-45.
10. WU, Z., HUANG, D. and WANG, W. Optimization for fire performance of ultra-low density fiberboards using response surface methodology, *BioResources*, 2017, **12**, (2), pp 3790-3800.
11. SUN, Z.G., XIAO, S.D. and XU, M.H. Optimization of the structure of water axial piston pump and cavitation of plunger cavity based on the Kriging model, *J Vibroengineering*, 2016, **18**, (4), pp 2460-2474.
12. AKHTAR, T. and SHOEMAKER, C.A. Multi objective optimization of computationally expensive multi-modal functions with RBF surrogates and multi-rule selection, *J Global Optimization*, 2016, **64**, (1), pp 17-32.
13. MULLUR, A.A. and MESSAC, A. Extended radial basis functions: More flexible and effective metamodeling, *AIAA J*, 2005, **43**, (6), pp 1306-1315.
14. CHEN, Z., QIU, H. and GAO, L. A local adaptive sampling method for reliability-based design optimization using Kriging model, *Structural & Multidisciplinary Optimization*, 2014, **49**, (3), pp 401-416.
15. REMONDO, D., SRINIVASAN, R. and NICOLA, V.F. Adaptive importance sampling for performance evaluation and parameter optimization of communication systems, *IEEE Transactions on Communications*, 2000, **48**, (4), pp 557-565.
16. LI, T.M., WU, Y.T. and CHUANG, Y.Y. SURE-based optimization for adaptive sampling and reconstruction, *ACM Transactions on Graphics*, 2012, **31**, (6), pp 1-9.
17. VYTLA, V.V.S., HUANG, P. and PENMETSA, R. Multi-objective aerodynamic shape optimization of high speed train nose using adaptive surrogate model, *AIAA Applied Aerodynamics Conference*, 2010, **15**, pp 25-34.

18. GOLZARI, A., SEFAT, M.H. and JAMSHIDI, S. Development of an adaptive surrogate model for production optimization, *J Petroleum Science & Engineering*, 2015, **133**, (6), pp 677-688.
19. JONES, D. R., SCHONLAU, M. and WELCH, W. J. Efficient global optimization of expensive black-box functions. *J Global Optimization*, 1998, **13**, (4), pp 455-492.
20. ZHANG, J.J., XU, L.W. and GAO, R.Z. Multi-island genetic algorithm opetimization of suspension system, *Telkomnika Indonesian J Electrical Engineering*, 2012, **10**, (7), pp 1685-1691.
21. GUO, S.Z., ANG, H.S. and CAI, H.M. Construction of an adaptive sampling surrogate model and application in composite material structure optimization, *Acta Materiae Compositae Sinica*, 2018, doi:10.13801/j.cnki.fhclxb.20170904.003.
22. PENG, F., WU, Z.Z. and YI, Z. Influence of sampling point distribution in freeform surfaces fitting with radial based function model, *Optics & Precision Engineering*, 2016, **24**, (7), pp 1564-1572.

https://doi.org/10.1017/aer.2018.40 Published online by Cambridge University Press